TWENTY-FIFTH EUROPEAN ROTORCRAFT FORUM

Paper n° C8

ICE ACCRETION CALCULATION ON HELICOPTER COMPONENTS

BY

G. MINGIONE, V. BRANDI
CIRA, ITALY

A SAPORITI
AGUSTA, ITALY

SEPTEMBER 14-16, 1999
ROME
ITALY

ASSOCIAZIONE INDUSTRIE PER L'AEROSPAZIO, I SISTEMI E LA DIFESA
ASSOCIAZIONE ITALIANA AERONAUTICA ED ASTRONAUTICA

ICE ACCRETION CALCULATION ON HELICOPTER COMPONENTS

Giuseppe Mingione[§] and Vincenzo Brandi[‡]
CIRA, Italian Aerospace Research Center
Via Maiorise, 81043 Capua (CE), Italy

A. Saporiti[†]
Agusta - Viale Agusta, 520
21017 Cascina Costa di Samarate (VA), Italy

The CIRA ice accretion code has been adapted for calculation of 3D ice accretion on helicopter components (HELICE code). The 3D ice accretion simulation is performed by calculating the aerodynamic flow field, the impingement region, the heat transfer coefficient and, finally, the ice shape. The modular code structure allows to easily interface the impingement module with different kinds of 3D flow solver; both field and boundary element methods can be used. In order to calculate the water impingement, an optimized 3D time-reducing droplet trajectory evaluation algorithm has been developed. An effective procedure has been adopted in order to evaluate the impingement area on the body surface. The boundary layer integral quantities as well as the ice thickness have been evaluated on the inviscid streamline pattern. At this aim, the well-known Messinger model has been employed on the surface bounded by two contiguous streamlines, taken as the water run-back path. Ice accretion on helicopter components, such as radomes, air intakes and rotor blades has been calculated.

1. Introduction

During the last years, from the beginning of the early 90's, many researchers from various institutions have tried to face the simulation of 3D ice shapes.

Among these efforts, the NASA researchers, Potapczuk and Bidwell, began, first of all, to extend the 2D simulation to 3D wing [1,2]. At these initial efforts, others followed also with the contribution of European researchers, such as Hedde and Guffond (Onera) who not only extended the Messinger model to 3D configurations[3] but they also tried to improve the Messinger ice accretion model by simulating some specifically 3D effects on the ice accretion, like the 'lobster tails' phenomenon[4].

All these efforts were limited to analyze fixed aircraft components while icing has historically been a problem especially for the rotating helicopter components. In fact, rotor systems are very sensitive to icing because of high accretion rates and mechanic vibration associated with asymmetric shedding.

Most helicopters (military and civilian) have restricted or no clearance for operation in forecasted icing conditions. One of the major reasons for this is the prohibitive cost of qualification/certification. Current procedures for certification are based on very expensive full scale flight testing in natural icing conditions[5] or on equivalent scaled wind tunnel tests[6]. Thus, there is a need to develop validated less expensive alternatives to the previous means to reduce certification costs.

In this scenario, CIRA has developed a theoretical model to calculate the ice accretion on 3D complex geometry. The theoretical estimation, when validated, can reduce the wind tunnel icing test number, so that the certification costs will significantly become lower.

---

§ Research Engineer, Aerodynamic & Propulsion Dept., Applied Aerodynamic Group.
‡ Research Engineer, Aerodynamic & Propulsion Dept., Applied Aerodynamic Group.
† Design Engineer, Aeromechanics Dept. Aerodynamics Group.

In this paper a general description of the simulation strategy with a particular emphasis on the modifications performed for helicopter applications (non-inertial forces, streamlines divergence-convergence) will be given. Some peculiar applications on fixed helicopter components, such as the cockpit nose and the air intake and on rotating component such as the helicopter rotor blades, will be shown.

2. An outline of the 3D ice accretion code

The general approach for 3D ice accretion model is similar to the one followed in the past by CIRA in 2D models[7] ,even if all steps in the procedure are complicated by the existence of the third spatial dimension; it consist in:

a) evaluation of the aerodynamic flow field around the body;
b) impingement region calculation through a Lagrangian approach;
c) ice thickness estimation through the Messinger model.

Here the modifications implemented on the basic 3-D impingement coefficient and ice accretion calculation module to face the complex 3-D rotorcraft geometry will be described; for further details, the readers can refer to previous publications [7, 8].

2.1 Impingement calculation

Once the aerodynamic flow field has been evaluated, different approaches can be used to compute the water impingement of the body. Some researchers use an Eulerian approach[9], where an air-water two-phase flow is modeled. To overcome the computational difficulties and to increase the flexibility of the code, CIRA has preferred to employ the classical Lagrangian approach where 3D droplet trajectories are calculated. To calculate droplets impingement on a rotating element such as a rotor blade, a blade fixed reference frame will be used to eliminate the time dependence from the flow field solution. Therefore, since the blade fixed reference system is non-inertial, the apparent forces must be taken into account. The droplet trajectory equations in a reference frame rotating at an angular velocity ω can be expressed as:

$$\sum_i \mathbf{F}_i = m\left(\ddot{\mathbf{r}} + 2\boldsymbol{\omega}\times\dot{r} + \boldsymbol{\omega}\times\boldsymbol{\omega}\times\mathbf{r}\right) \qquad (1)$$

where $\mathbf{r}=[x,y,z]^T$ is the trajectory point position vector, $\mathbf{F}_i$ is the sum of all the forces acting on the particle.

The main acting forces are the aerodynamic and the gravity ones, since the other contributions (Basset unsteady history term, buoyancy) can be considered negligible.

$$\sum_i \mathbf{F}_i = \mathbf{D} + \mathbf{G}$$

The aerodynamic drag depends on the droplet relative velocity with respect to the air and, supposing ω parallel to the z axis and $U_r = V_d - V_a$ as slip velocity module, the vectorial equation (1) can be projected on the reference axis, thus obtaining three algebraic equations:

$$\begin{cases} \left(\frac{1}{2}\rho C_D S U_r^2\right)_x + mg_x = m(\ddot{x} - 2\omega\,\dot{y} - \omega^2 x) \\ \left(\frac{1}{2}\rho C_D S U_r^2\right)_y + mg_y = m(\ddot{y} + 2\omega\,\dot{x} - \omega^2 y) \\ \left(\frac{1}{2}\rho C_D S U_r^2\right)_z + mg_z = m\ddot{z} \end{cases} \qquad (2)$$

The droplet starting velocity must satisfy the free stream conditions, i.e. the no-slip condition between droplet and air; since the air velocity is not uniform through the field also the droplet velocity depends on the position and can be expressed as $V_a=\omega\times r$.

The droplet trajectory equations (2) have been integrated by means of the 4th order Runge-Kutta method with an adaptive step-size control algorithm which let the step be inversely proportional to the velocity gradient.

Therefore, the air flow velocity is required to calculate the droplet trajectories. It can be obtained through an interpolation from the

velocity values available on the corners of a spatial off-body grid. In this way, different flow solvers can be interfaced with the trajectory module. Both field methods (full potential, Euler, Navier-Stokes) and boundary element methods (panel methods) can be employed so allowing each user to adopt the available in-house aerodynamic flow solver.

The advantage of a field method is that the grid points, where the velocity values must be available, can be promptly those employed for the flow field solution while a panel method requires the definition of an off-body points grid and the additional calculation of the velocity into these points. In this latter case the advantage is that the grid refinement is more controlled and oriented to the improvement of the velocity interpolation accuracy. In fact, being the air velocity obtained through an interpolation, the grid refinement, especially around the surface where the impact points are evaluated, greatly affects the result accuracy. In addition off-body points can be distributed in a number of blocks, each one with a different grid refinement, so that the user can build up different grids according to the separation distance from the body (finer in the near field, coarser in the far field). The grid extension in the field must be large enough to make the upstream droplet starting conditions close to the free stream ones.

The impingement coefficient is calculated as the ratio between the area bounded by the trajectories which leaves from four starting points at free stream conditions, A_{start}, and the target area caused by the correspondent impact points, A_{surf}:

$$\beta = \frac{A_{start}}{A_{surf}}$$

Once the impact points are determined, a surface oriented (ξ,η) co-ordinate system is defined and a Jacobian matrix is built to allow the transformations between the surface oriented 2-D (ξ,η) and the physical 3-D Cartesian co-ordinate systems. The surface oriented (ξ,η) co-ordinate system allows an easier impingement coefficient calculation, allowing to more correctly define the surface area through the following expression:

$$A_{surf} = \int_B \sqrt{J_1^2 + J_2^2 + J_3^2}\, d\xi d\eta$$

where J_1, J_2, J_3, are the $e_\xi \wedge e_\eta$ vector product components on the (x,y,z) global Cartesian reference frame, B is the reference domain of the curvilinear surface-oriented (ξ,η) co-ordinates, while e_ξ and e_η are computed, following a common practice, as the derivative of the Cartesian components with respect the new co-ordinates.

Moreover, once the contro-variant velocity components along the surface reference system (U_ξ, U_η) have been evaluated, a quicker and easier surface streamline calculation can be carried out with the following expression:

$$\frac{h_\xi d\xi}{h_\eta d\eta} = \frac{U_\xi}{U_\eta}$$

where h_ξ and h_η are the scale factors of the generalized surface co-ordinate system with respect the Cartesian one.

2.2 Boundary Layer and Ice accretion calculation

The water run-back path is assumed to follow the inviscid streamline. Therefore, a new streamline fitted co-ordinate system is defined and the Messinger model is applied to calculate the ice thickness and the run back fluxes in cells that are confined between two contiguous streamlines. Prior to apply the ice accretion model, whose detailed description is reported in reference [7], some words must be dedicated to the boundary layer method employed when 3D geometries have to be taken into account. In fact, in order to apply the ice accretion model, the convective heat transfer coefficient is to be known, because it represents one of the most important contributions to the ice accretion rate.

In 2D and quasi-2D flow patterns, such as, for example, a swept wing with a very large aspect ratio, the 2D boundary layer calculation applied in ref. [7], provides a sufficient approximation. When the flow field is essentially 3D, with significant streamlines convergence and divergence, such as in the case of a fuselage, an intermediate step between 2D and full-3D calculations is the Cooke analogy (analogy between axisymmetric and full three dimensional boundary layer [10]).

With the assumption that within the boundary layer the velocity normal to the external streamlines (crossflow) is small if compared to the velocity in the streamline direction, Cooke demonstrated that the streamwise momentum, energy and continuity equations reduce to those valid for flows over an equivalent asymmetric body whose radius is in each point related to the streamlines divergence or convergence.

The result of the Cooke analogy hypothesis is that the boundary layer streamwise equations are not coupled with the boundary layer crossflow equations and can be solved independently. This theory directly applies to the laminar compressible or incompressible flows; the same theory was successfully applied also by other authors[11], both for laminar and for turbulent boundary layers.

The 2D Karman equation valid for laminar or turbulent boundary layer is:

$$\frac{d\theta}{ds}+\overbrace{\frac{dU_e}{ds}(H+2)\frac{U_e}{\theta}}^{1}=\frac{C_f}{2}$$

The axisymmetric version of this equation appears as the above unless a new term added at the left hand side of the equation:

$$\frac{d\theta}{ds}+\overbrace{\frac{dU_e}{ds}(H+2)\frac{U_e}{\theta}}^{1}+\overbrace{\theta\frac{1}{r}\frac{dr}{ds}}^{2}=\frac{C_f}{2} \quad (3)$$

The term limited with the bracket 1 represents the pressure gradient correction with respect to the equation, valid for a flat plate flow, while the second bracketed term (spreading factor) takes into account the 3D effects (body curvature).

For an axisymmetric body surface, streamlines follow the body meridians line (lines obtained from the intersection of the body with a plane passing through the symmetry axis). If the meridian lines are described by the radius variation with respect to the curvilinear abscissa (s) measured along the meridian line, the term 2 in the equation (3) can be easily calculated. No cross-flow would exist along the circumferential direction.

For a non axisymmetric body, streamlines can significantly differ from the meridian line, but the streamline spreading factor can always be defined by replacing the meridian lines with the streamlines. Therefore, a convenient surface co-ordinates reference frame to study the 3D integral boundary layer equations is the so called "streamline co-ordinates".

One can suppose that a new curvilinear orthogonal co-ordinate system (ξ,η) can be defined for the boundary layer calculation and for the ice accretion thickness evaluation purpose, so that the curves of intersection of the surface η=const with the body surface (ζ=0) are surface streamlines.

In this system, the stream-wise momentum equation can be written as:

$$\frac{d\theta}{d\xi}+\overbrace{\frac{dU_e}{d\xi}(H+2)\frac{U_e}{\theta}}^{1}+\overbrace{\theta\frac{1}{h_\eta}\frac{dh_\eta}{d\xi}}^{2}=\frac{C_{f_\xi}}{2} \quad (4)$$

This equation describes the development of the stream-wise momentum thickness θ along the streamline co-ordinate ξ, which is here computed as the actual curvilinear abscissa measured along the streamline (h_ξ=1).

The term 2 in equation (4) is similar to the term 2 in equation 3, valid for the axisymmetric flows; it represents the streamline curvature contribution, i.e. it takes into account the possibility that two

contiguous streamlines can converge or diverge. In Figure 1, an example of converging and diverging streamlines is reported.

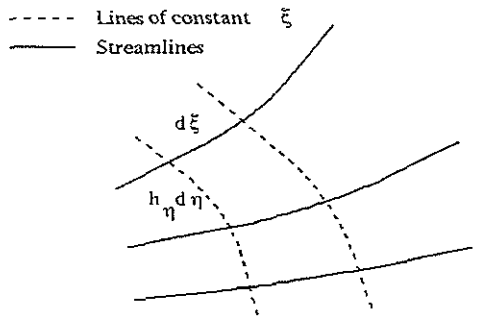

Diverging Streamlines

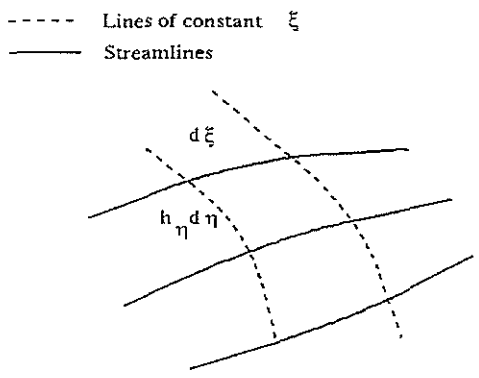

Converging Streamlines

Figure 1: Diverging and converging streamlines

The equation (4) can be solved in the laminar part of boundary layer with the well-known Thwaites method.

The streamline curvature correction term h_η directly appears in the momentum thickness expression:

$$\theta^2 = \frac{\nu a}{U_e^b h_\eta^{\,2}} \int_o^s U_e^{b-1} h_\eta^{\,2} ds + \frac{(h_\eta^{\,2}\theta^2 U_e^b)_0}{h_\eta^{\,2} U_e^b}$$

Different values of the a and b coefficients characterize the different versions of the Thwaites method (the classical version is a=0.45 and b=6 even if frequently used values are a = 0.414, b = 5.68).

The heat transfer coefficient, h, can be calculated with the Spalding analogy, with the correction due to the streamline curvature. Starting from the conductive thickness expression:

$$\delta_c^2 = \frac{\nu A}{U_e^B h_\eta^{\,2}} \int_o^s U_e^{B-1} h_\eta^{\,2} ds + \frac{(h_\eta^{\,2}\delta_c^2 U_e^B)_0}{h_\eta^{\,2} U_e^B}$$

the h value assume the following form:

$$h = \frac{k_c}{\delta_c}$$

For a turbulent flow, once a suited expression for Cf is adopted, the following expression for the momentum thickness is obtained by integrating the (4):

$$\theta^{5/4} = \frac{.016\nu^{1/4}}{U_e^{35/8} h_\eta^{5/4}} \int_o^s U_e^{33/8} h_\eta^{5/4} ds + \frac{(h_\eta^{5/4}\theta^{5/4} U_e^{35/8})_{tr}}{h_\eta^{5/4}\theta^{35/8}}$$

Once calculated the turbulent momentum thickness, the Cf and therefore the heat transfer coefficient, h, can be evaluated from the momentum thickness and the roughness, k by using the same expression as in [7] for 2D flows.

Once the boundary layer calculation has been carried out, the Messinger ice accretion model can be applied between two contiguous streamlines. Therefore the ice thickness is first evaluated on panel centroid points and then interpolated into the corner geometry point to build the iced geometry.

3. Applications to helicopter components

Even if ice accretion on an aircraft or rotorcraft radome does not have a relevant aerodynamic effect, it can have a detrimental effect on the aircraft weight and on the radar performances (usually installed in the radome).

The first HELICE application has been the evaluation of the impingement level and the ice accretion on a typical rotorcraft nose.

3.1 Rotorcraft nose ice accretion

The following aerodynamic and water droplet characteristics have been assumed:

- Mach = 0.225
- Angle-of-attack = 0°
- Monodispersed droplet distribution with MVD = 50 μm
- T_∞= 255 K
- LWC = 1.03 g/m^3
- accretion time =390 sec

The aerodynamic calculation has been performed by Agusta using the VSAERO 3D panel code.

In Figure 2, the impingement level on the nose is shown.

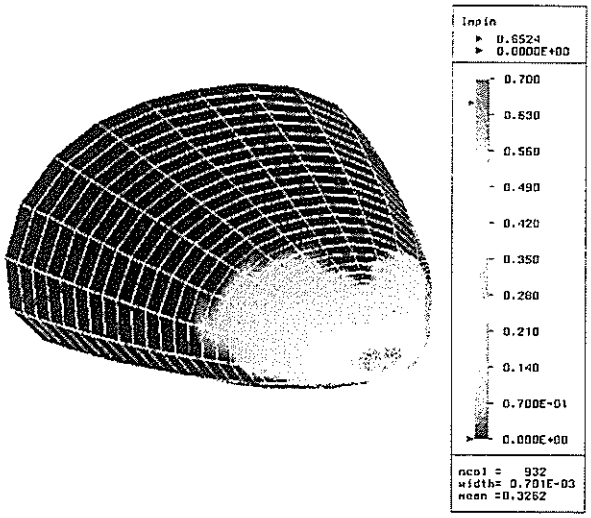

Figure 2: Impingement level

As expected, the impingement level has reached the maximum value near the leading edge .

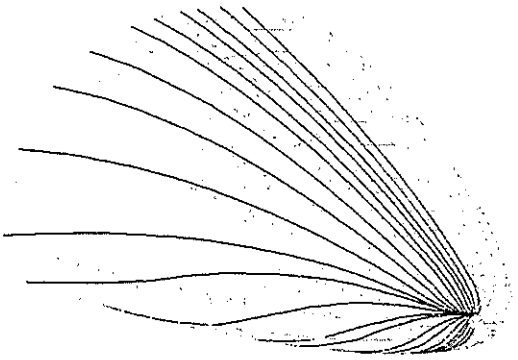

Figure 3: Streamline pattern

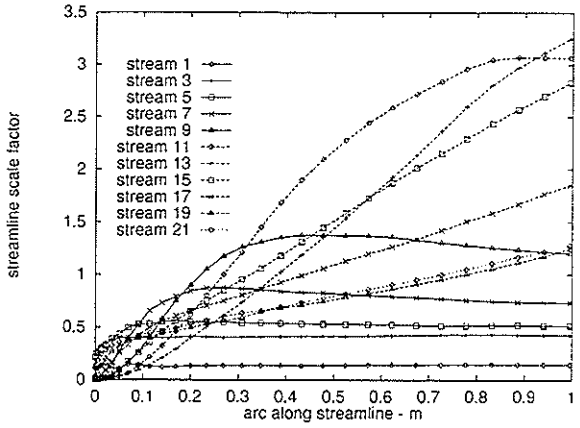

Figure 4: Spreading factor on selected streamlines

Surface streamline have been calculated and are plotted in figure 3. By choosing with accuracy the starting points, all the fuselage can be uniformly covered.

In Figure 4, the streamline metric coefficient h_η is plotted. This term directly affects the momentum thickness development, taking into account the 3D effects, i.e., the convergence or divergence of the streamline (eq. 4).

In Figure 5, the curvature of the ξ = const curve is plotted. This represents the third factor of the equation (4); therefore whereas this term is negligible, the 2D model can work well. As expected this term vanishes as the streamline moves toward the rear part of the fuselage, where the body radius increases. The streamlines which are traced around the symmetry plane (stream 3 upper and stream 21 lower in Figures 4 to 6) are less affected by the Cooke correction term. The corrected momentum thickness, Figure 6, is comparable to the 2D momentum thickness. The difference between corrected and pure 2D calculation are more evident if we refer to the heat transfer coefficient (Figure 7). The corrected heat transfer, is always larger than the pure 2D heat transfer even if the difference is larger on the fuselage side.

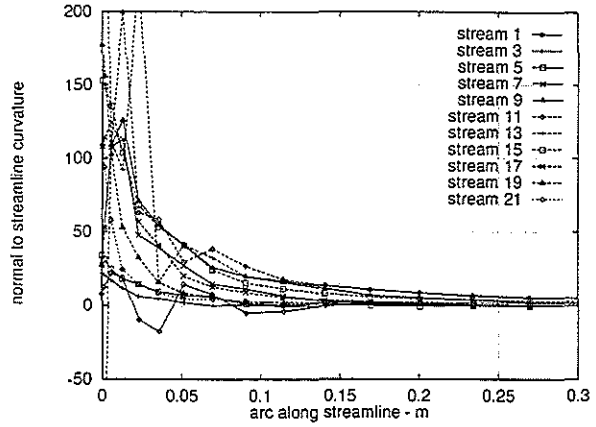

Figure 5: Streamline curvature correction term (see Eq. 5).

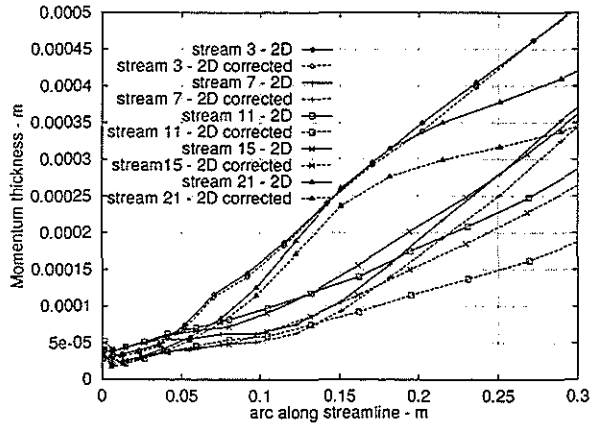

Figure 6: Comparison between 2D and 2D corrected momentum thickness development on selected streamline.

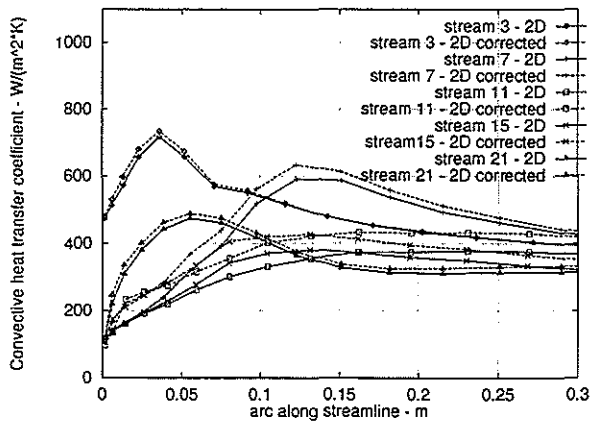

Figure 7: Comparison between 2D and 2D corrected convective heat transfer coefficient on selected streamline

In Figure 8 and Figure 9, the ice accretion on the symmetry plane, calculated with different boundary layer models can be seen.

The ice thickness with the 2D corrected model is a little bit larger than the one calculated with the 2D theory. Taking into account that in the symmetry plane the difference between the two models should be less evident, for other sections the Cooke correction could provide a more evident effect.

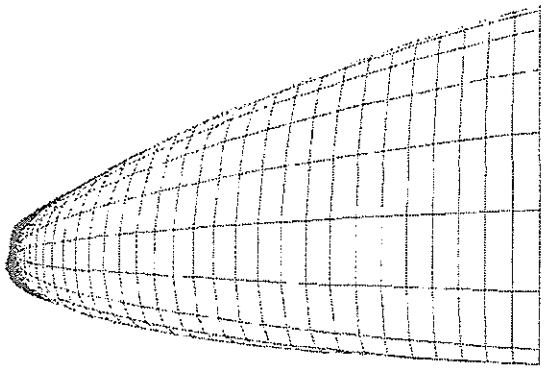

Figure 8: Ice accretion in the vertical plane (2D corrected BL method)

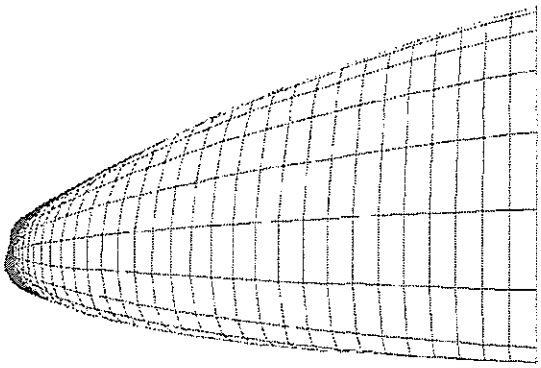

Figure 9: Ice accretion in the vertical plane (2D BL method)

3.2 Rotorcraft air-intake

One of the concerns during rotorcraft design and certification is the possibility that the air-intake Foreign Object Damage protection grid can be choked by ice accumulation. At this end the collection efficiency and the ice accretion has been evaluated on a generic air intake FOD protection grid.

In this case the surface, where the collection efficiency has to be calculated, is not perpendicular to the main flow direction (see the sketch in Figure 10). Even if this lay-out is very complicated, the flow field is complex and deformed by the rotor influence and the limiting trajectories are more cumbersome to find, the code proved to be able to manage this complex pattern.

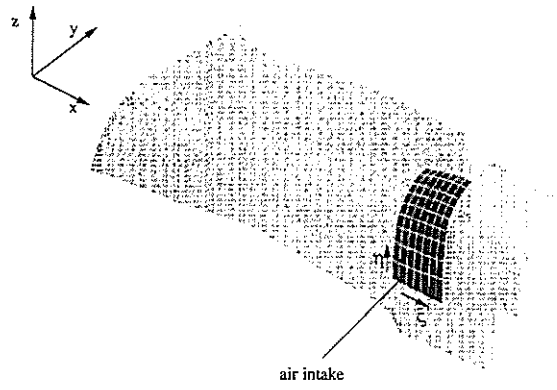

Figure 10: Air intake layout

The tested aerodynamic condition referred to a climb flight situation with the addition of a yaw flight angle, the rotor effects have been included in the simulation and the flow analyzed by Agusta using the VSAERO panel code.

- Mach = 0.104
- Angle of attack, α = - 23.6 degrees
- Yaw angle = - 20 degrees
- Monodispersed droplet distribution with MVD = 20 μm.

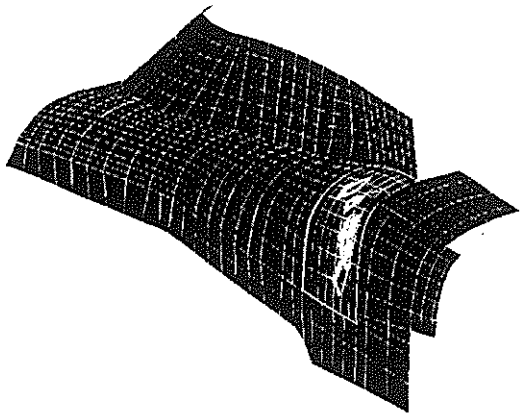

Figure 11: Air intake: impingement contour map

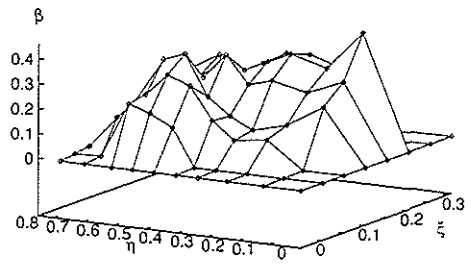

Figure 12: Air intake: impingement level

The impingement calculation results are reported in Figure 11 and Figure 12. In the former picture the impingement contour map is shown while in the latter the numerical level is plotted. The ξ and η labels refer to the curvilinear directions along the intake borders.

Figure 13: Ice accretion on the air intake FOD grid

While the impingement coefficient on the grid provides an indication of location and amount of collected water, only an ice accretion calculation can provide more quantitative data to understand if ice is going to chock the grid. At this end a procedure based on the 3D correction of Langmuir and Blodget theory has been used to calculate the ice accretion on the FOD protection grid [8].

The ice accretion has been calculated at the same conditions used to calculate the local collection efficiency, assuming a grid diameter of 2 millimeters and:

- LWC = 0.6 g/m^3
- Time accretion = 1800 sec

In Figure 13, for clearness of representation, only a limited number of grid elements and the ice accretion at a limited number of stations are reported. The procedure used can provide an indication of the size and the shape of the ice accretion. The maximum ice accretion thickness ranges from 0 to 1÷2 millimeters. It is clear that the predominant ice shape dimension is the horizontal one, meaning that for this case, even if there is an important vertical contribution to local velocity from the rotor, the preferential direction is the horizontal one.

3.3 Application to a typical rotor blade

Finally ice accretion has been calculated on a typical propeller blade in hovering. Even if the hover condition is simpler than the forward flight conditions because the flow is steady, some complex feature like rotation effects and strong 3-D effects must still be taken in account.

The flow field has been calculated using the code HELIFP (HELIcopter Full Potential) that is a CFD code for the prediction of flows around isolated helicopter blades (of arbitrary planform) in hover or forward flight based on the unsteady conservative full potential equation with entropy correction, finite volume discretization and internal Newton iterations in Approximate Factorization (AF) numerical scheme. HELIFP was developed within the framework of the Brite/EuRam HELISHAPE Project (1993-1996) and it is the first common European CFD code accomplished by seven different organizations: CIRA (IT), DERA (UK), ONERA (FR), NLR (NL), Polit. of Milan (IT), AGUSTA (IT) and GKN-WESTLAND (UK).

The following conditions were investigated:

- Span = 1.045 m
- Chord = .0762 m
- M_{tip}= 0.8
- Angle-of-attack = 0°
- Monodispersed droplet distribution with MVD = 20 μm
- T_∞= 265 K
- LWC = .3 g/m^3
- accretion time = 30 sec

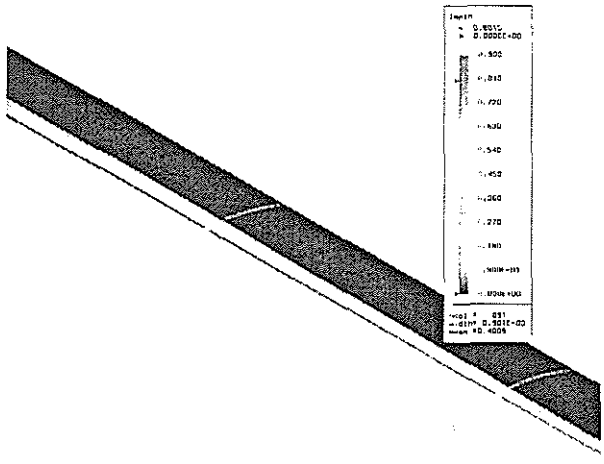

Figure 14: Trajectories and impingement level on rotor blade in hovering.

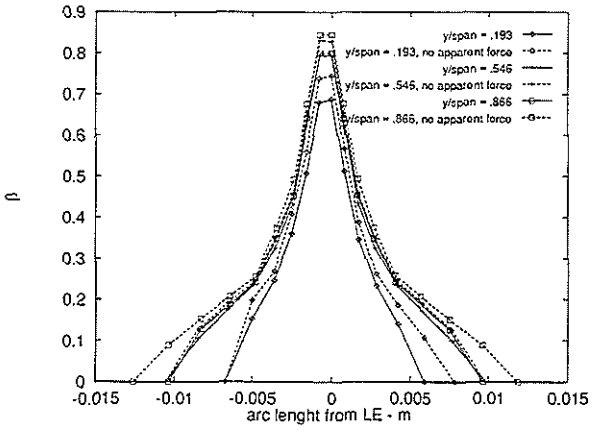

Figure 15: Comparison between the collection efficiency with and without the apparent forces.

The droplet trajectories (Fig. 14) have been calculated once including and once excluding

the non-inertial term in the trajectory equations (fig. 15). Even if the magnitude of the non-inertial terms depends on entity of the blade angular velocity, in this case we can see that the effect is a small reduction of the collection efficiency (Fig. 15).

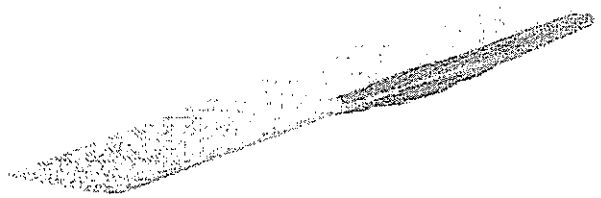

Figure 16: Ice accretion along the span with $T_\infty = 265$ K

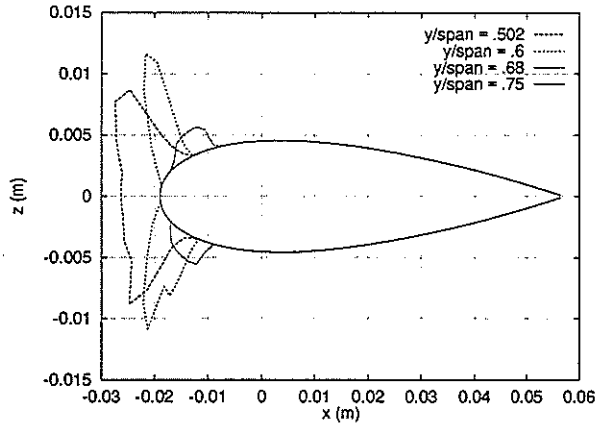

Figure 17: Ice accretion along the span with $T_\infty = 265$ K

Finally ice accretion has been calculated (Fig. 16), and shapes at different location along the blade have been compared. The ice shapes seem to be rime near the blade root, where the local Mach number is lower and therefore the kinetic heating is lower. As we approach the blade tip, the ice shape tends to pass from rime to glaze, and finally no ice at all is present at the most external part of the blade. Even if a detailed comparison with experimental data has not been possible, this behavior seems to qualitatively reflect the experimental data for similar configurations[14].

4. Conclusions

In this paper the 'HELICE' 3D ice accretion code has been presented. The code can evaluate the water collection efficiency and ice accretion also on complex geometry and on rotating aircraft components (e.g. rotor or propeller blades) and can be interfaced with different flow solvers. A blade fixed reference frame is used and non-inertial forces have been taken into account. An automatic procedure for the identification of impinging and limiting trajectories has been implemented. The ice accretion has been calculated using either the Messinger model or the 3D effects upgraded Langmuir and Blodget procedure depending on the test case typology.

To demonstrate the code capabilities, impingement coefficient and ice accretion have been calculated on some typical ice sensible rotorcraft components.

5. Acknowledgements

The authors would like to acknowledge Antonio Pagano, for his suggestions and his help in providing the HELIFP aerodynamic solution, required for the propeller blade impingement and ice accretion calculation.

6. References

[1] M.G. Potapczuk, C.S. Bidwell, "Swept wing ice accretion model", AIAA-90-0756 Reno, Nevada, January 1990

[2] M.G. Potapczuk, C.S. Bidwell, "Numerical simulation of ice growth on a MS-317 swept wing geometry", AIAA-91-0263 Reno, Nevada, January 1991

[3] T. Hedde, D. Guffond, "Development of a three-dimensional icing code, comparison with experimental shapes" AIAA 92-0041 Reno, Nevada, January 1992

[4] T. Hedde, D. Guffond, "Improvement of the ONERA 3D icing code. Comparison with 3D experimental shapes" AIAA 93-0169 Reno, Nevada, January 1993

[5] J. Tracy and D. J. Rowley, "Development and Certification of the EH101 for Operation in Natural Icing", International Icing Symposium, 1995, September 18-21

[6] R. K. Britton, T. H. Bond and R. J. Flemming, "An overview of a Model Rotor Icing Test in the NASA Lewis Icing Research Tunnel", AIAA 94 0716, Reno, NV, January 10-13, 1994 (also NASA TM 106471)

[7] G. Mingione and V. Brandi "Ice Accretion Prediction on Multielement Airfoils", *Journal of Aircraft*, Vol. 35, No. 2, March-April 1998

[8] V. Brandi "IMPIN3D: a code for the evaluation of water droplet impingement on 3D geometry", CIRA-TN-98-214, December 1998

[9] Y. Bourgault, W.G. Habashi, J. Dompierre, Z. Boutanios, W. Dibartolomeo "An Eulerian Approach to supercooled droplets impingement calculations" AIAA 97-0176, Reno, Nevada, January 1997

[10] J. C. Cooke, "An Axially Symmetric Analogue for General Three-Dimensional Boundary Layers.", R. & M. No. 3200, British A. R. C., June, 1959.

[11] H.H. Hamilton and K.J. Weilmuenster, "Application of Axisymmetric Analogue for calculating Heating in Three-Dimensional Flows", AIAA 85-0245.

[12] Nathman, J.K., "VSAERO, A Computer Program for Calculating the Non-linear Aerodynamic Characteristics of Arbitrary Configurations", User's Manual Version 6.0, November 1997

[13] M. Costes, J.C. Le Balleur, L. Gasparini, L. Vigevano, M.H.L. Hounjet, A. Kokkalis, J.V. Miller, M. Spruce, A. Pagano, P. Renzoni, A. Rocchetto, F. Toulmay, "Development of a Common European Unsteady Full Potential Code for Helicopter Rotors in Hover and Forward Flight", American Helicopter Society 53rd Annual Forum,Virginia Beach, Virginia, April 29-May 1, 1997.

[14] D.P. Guffond "Icing and De-Icing Test on a ¼ Scale Rotor in the ONERA s1MA wind tunnel", AIAA-86-0480